

Magnetic-field dependence of the cross section for m_J mixing in $^2P_{1/2}$ Cs and Rb atoms

W. Kedzierski, Ju Gao, W. E. Baylis, and L. Krause

Department of Physics, University of Windsor, Windsor, Ontario, Canada N9B 3P4

(Received 10 November 1993)

Transitions between the Zeeman substates of Cs $6^2P_{1/2}$ and Rb $5^2P_{1/2}$ atoms, induced in collisions with He atoms, have been investigated experimentally by methods of atomic fluorescence spectroscopy. The collision process has also been studied theoretically with time-dependent perturbation theory. Cs or Rb vapor contained in a quartz cell together with helium at low pressure was selectively excited by pulsed dye-laser radiation to the $^2P_{1/2,-1/2}$ Zeeman substate in a magnetic field ranging from 1.5 T to 7 T. The fluorescence spectrum, consisting of components emitted from the directly excited state and from the collisionally populated state, was resolved with a Fabry-Pérot interferometer. Measurements of the relative intensities of the fluorescence components yielded the Zeeman mixing cross section for Cs-He and Rb-He collisions. It was found that the Cs $6^2P_{1/2}$ cross section varied approximately as B^2 in the range $0 < B < 0.76$ T, showed a much weaker field dependence in the range from 0.76 T to 5 T, where it peaked, and declined slightly at $B > 5$ T. The Rb $5^2P_{1/2}$ cross section did not exhibit any variation with B . A theoretical calculation of the Cs cross section carried out using time-dependent perturbation theory explains the magnetic-field enhancement in terms of the minute magnetic-field-induced mixing of the $P_{1/2}$ and $P_{3/2}$ states and the resulting breaking of time-reversal symmetry. The results of the calculation are in good agreement with the experimental results at fields in the range $0 < B < 5$ T.

PACS number(s): 34.50.-s, 32.50.+d

I. INTRODUCTION

The orientation and alignment of excited atoms, as well as the collisional relaxation and transfer of atomic multipole moments, have been the subject of several recent experimental investigations [1]. For example, the processes $^2P_{1/2,m_J} \leftrightarrow ^2P_{3/2,m'_J}$ in the Na resonance state were studied by Kimura *et al.* [2], in 5^2P K atoms by Berends, Kedzierski, and Krause [3], and in 6^2P Rb atoms by Kedzierski, Middleton, and Krause [4]. The process $^1P_{1,m_J} \rightarrow ^3P_{2,m'_J}$ in Ba, induced in collisions with some diatomic molecules, was investigated by Mestdagh *et al.* [5], and the alignment-to-orientation conversion in sodium by Han and Schinn [6]. There has also been some interest in exploring the effect of a magnetic field on m_J mixing rates (or cross sections) in Na [7] and Hg [8] and, more recently, in Ne, where the magnetic-field dependence of collisional disalignment rates was investigated in fields up to 10 T [9].

In this investigation we report the results of experiments in which we excited one of the two m_J Zeeman substates of $6^2P_{1/2}$ cesium atoms and $5^2P_{1/2}$ rubidium atoms in magnetic fields up to 7 T, and followed the transfer of population to the other m_J substate, induced by He collisions. Since both the alkali-metal vapor pressures and the He pressures were kept low, effects due to trapping of resonance radiation were negligible as was the collisional $^2P_{1/2}-^2P_{3/2}$ mixing and Zeeman mixing by collisions with ground-state alkali-metal atoms. The resulting Zeeman fluorescence spectrum consisting of just two components was resolved with a Fabry-Pérot interferometer and measurements of the relative intensities yielded the m_J mixing cross sections in relation to the magnetic-

field strength. In order to verify the observed effects, we also carried out an independent and fairly extensive calculation that indicated the variation of the Cs $^2P_{1/2}$ cross sections with the field strength and permitted a comparison with the experimental results. This work follows an earlier study of the Cs $^2P_{1/2}$ disorientation cross section over a much smaller range of magnetic fields [10], the results of which are found to match well with those reported below.

II. THEORY

A. Collisions of oriented alkali-metal $^2P_{1/2}$ atoms with ground-state He atoms in a magnetic field

An explanation for the affect of the magnetic field on the Cs $6^2P_{1/2}$ Zeeman mixing cross section was proposed by Baylis [1] who suggested that magnetic-field-induced (virtual) $^2P_{1/2}-^2P_{3/2}$ mixing enhances the Zeeman mixing rate. We now explore this model further using time-dependent perturbation theory (TDPT).

The Hamiltonian, describing a collision process in the presence of a magnetic field, may be written

$$H = H_0 + \mu_0(2\mathbf{S} + \mathbf{L}) \cdot \mathbf{B} + V(t), \quad (1)$$

where H_0 is the atomic Hamiltonian in the absence of the field \mathbf{B} , and $V(t)$ represents the collisional interaction between the alkali-metal and He atoms; \mathbf{L} and \mathbf{S} are the orbital and spin angular momenta of the alkali-metal valence electron, respectively, and μ_0 is the Bohr magneton. \mathbf{B} is assumed to be sufficiently weak to be treated as a perturbation and sufficiently strong to decouple the nuclear spin \mathbf{I} from the electron angular momentum \mathbf{J} , so

that hyperfine structure need not be considered [11]. In the ${}^2P_{1/2}$ state, nuclear-spin decoupling occurs around 0.02 T. The static part of the Hamiltonian, Eq. (1) less the collisional interaction, is

$$H_B = H_0 + \mu_0(2\mathbf{S} + \mathbf{L}) \cdot \mathbf{B} . \quad (2)$$

According to perturbation theory, the $P_{1/2}$ eigenstates of H_B are no longer pure $|j, m\rangle = |\frac{1}{2}, \pm\frac{1}{2}\rangle$ states, but also include small admixtures of the $P_{3/2}$ states of the same m_j values

$$|1\rangle = |\frac{1}{2}, -\frac{1}{2}\rangle - \alpha |\frac{3}{2}, -\frac{1}{2}\rangle , \quad (3)$$

$$|2\rangle = |\frac{1}{2}, \frac{1}{2}\rangle - \alpha |\frac{3}{2}, \frac{1}{2}\rangle , \quad (4)$$

where

$$\alpha = - \langle \frac{3}{2}, \frac{1}{2} | (2\mathbf{S} + \mathbf{L}) \cdot \mu_0 \mathbf{B} | \frac{1}{2}, \frac{1}{2} \rangle / \Delta E = \frac{\sqrt{2}}{3} \mu_0 \mathbf{B} / \Delta E . \quad (5)$$

The six ${}^2P_{1/2}$ and ${}^2P_{3/2}$ Zeeman substates constitute a basis set for our problem and ΔE is the ${}^2P_{1/2}$ - ${}^2P_{3/2}$ fine-structure (FS) splitting. All other states of the Cs or Rb + He system are relatively distant and may be ignored for the purpose of this argument. Accordingly,

$$H_B |1\rangle = E_1 |1\rangle , \quad (6)$$

$$H_B |2\rangle = E_2 |2\rangle , \quad (7)$$

and

$$E_2 - E_1 \approx \frac{2}{3} \mu_0 \mathbf{B} \ll \frac{\hbar}{\tau_c} \ll \Delta E , \quad (8)$$

where τ_c is the duration of the collision.

The Schrödinger equation in the interaction picture (IP), stated in atomic units, is

$$i \frac{d}{dt} \phi = \exp(iH_B t) V(t) \exp(-iH_B t) \phi = V^I(t) \phi , \quad (9)$$

where ϕ is any state in the IP. If the system is initially ($t = -\infty$) in state $|1\rangle$, the state $|t\rangle$ at time t may be written as follows from TDPT:

$$|t\rangle = \left[1 - i \int_{-\infty}^t dt_1 V^I(t_1) - \int_{-\infty}^t dt_1 \int_{-\infty}^{t_1} dt_2 V^I(t_1) V^I(t_2) + \dots \right] |1\rangle . \quad (10)$$

The probability of transition $|1\rangle \rightarrow |2\rangle$ is

$$P = |\langle 2|t\rangle|^2 . \quad (11)$$

The transition amplitude is obtained to second order from Eqs. (10) and (11):

$$\langle 2|t\rangle = \langle 2|1\rangle - i \int_{-\infty}^t dt_1 \langle 2|V^I(t_1)|1\rangle - \int_{-\infty}^t dt_1 \int_{-\infty}^{t_1} dt_2 \langle 2|V^I(t_1)V^I(t_2)|1\rangle . \quad (12)$$

The first term in Eq. (12) vanishes because of orthogonality,

and the second term, which represents the perturbation (to first order), contains the matrix element

$$\begin{aligned} \langle 2|V^I(t_1)|1\rangle &= \langle 2|\exp(iH_B t_1)V(t_1)\exp(-iH_B t_1)|1\rangle \\ &= \exp[i(E_2 - E_1)t_1] \langle 2|V(t_1)|1\rangle . \end{aligned} \quad (13)$$

From Eqs. (3) and (4),

$$\langle 2|V(t)|1\rangle = -2\alpha \langle \frac{3}{2}, \frac{1}{2}|V(t)|\frac{1}{2}, -\frac{1}{2}\rangle . \quad (14)$$

In writing Eq. (14) we used the relation representing "instantaneous" time-reversal symmetry [1]:

$$\begin{aligned} \langle j, m|V(t)|j, m'\rangle \\ = (-1)^{j-j'-m+m'} \langle j', -m'|V(t)|j, -m\rangle . \end{aligned} \quad (15)$$

Equation (15) leads to

$$\begin{aligned} \langle \frac{1}{2}, \frac{1}{2}|V(t)|\frac{3}{2}, -\frac{1}{2}\rangle &= \langle \frac{3}{2}, \frac{1}{2}|V(t)|\frac{1}{2}, -\frac{1}{2}\rangle , \\ \langle \frac{1}{2}, \frac{1}{2}|V(t)|\frac{1}{2}, -\frac{1}{2}\rangle &= \langle \frac{3}{2}, \frac{1}{2}|V(t)|\frac{3}{2}, -\frac{1}{2}\rangle = 0 . \end{aligned} \quad (16)$$

We note that the phase factor $\exp[i(E_2 - E_1)t_1]$ in Eq. (13) oscillates slowly because $(E_2 - E_1)$ is small, as stipulated by Eq. (8). Accordingly, compared to the second-order collisional contribution (see below), the contribution from $\langle 2|V(t_1)|1\rangle$ to the transition probability is not negligible even though the coupling constant α is small. This explains why a perturbative magnetic field can substantially enhance the m_j mixing cross section. The first-order perturbation probability may be expressed as

$$P^{(1)} = \left| \int_{-\infty}^{\infty} dt_1 \exp[i(E_2 - E_1)t_1] \langle 2|V(t_1)|1\rangle \right|^2 . \quad (17)$$

The integration of (17) is carried out by changing the variable t to \mathbf{R} , the interatomic coordinate. Using the straight-path approximation, the coordinates are related as follows:

$$\mathbf{R} = (b^2 + v^2 t^2)^{1/2} , \quad (18)$$

where b is the impact parameter and v is the relative speed of the collision partners, which is assumed constant during the collision. Thus $V(t)$ becomes $V(\mathbf{r}, \mathbf{R})$, where \mathbf{r} represents the intra-atomic coordinate. $V(\mathbf{r}, \mathbf{R})$ can be expanded in Legendre polynomials:

$$V(\mathbf{r}, \mathbf{R}) = \sum_L V_L(r, R) P_L(\hat{\mathbf{r}} \cdot \hat{\mathbf{R}}) . \quad (19)$$

By symmetry under spatial inversion and the triangular rule, only the $L=2$ terms contribute to the matrix element in Eq. (17), and the matrix element $V_{211}(\mathbf{R})$ of $V_2(r, R)$, between p -state wave functions, calculated in a pseudopotential calculation [12,13], can be reasonably well fitted by a power-law potential,

$$V_{211}(\mathbf{R}) = C_n R^{-n} , \quad (20)$$

where C_n is a constant and $n=5.46$ for the Cs-He interaction [12]. The integration (17) must be averaged over all orientations of the collision frame relative to the magnetic field, and the transition probability is obtained as a function of the impact parameter b

$$P(b) = \alpha^2 \frac{3}{5} \frac{n^2 - 3n + 3}{n^2} \left[\frac{2C_n}{5vb^{n-1}} \beta \left[\frac{1}{2}, \frac{n-1}{2} \right] \right]^2, \quad (21)$$

where β is the beta function [14]. For a given n , $P(b)$ reduces to

$$P(b) = \frac{\lambda B^2}{b^{n_1}}, \quad (22)$$

where $n_1 = 2(n-1)$ and λ is a constant:

$$\lambda = \frac{2}{9} \left[\frac{\mu_0}{\Delta E} \right]^2 \frac{3}{5} \frac{n^2 - 3n + 3}{n^2} \left[\frac{2\beta \left[\frac{1}{2}, \frac{n-1}{2} \right]}{5v} \right]^2 C_n^2. \quad (23)$$

Equation (23) was evaluated numerically using the following parameters (expressed in atomic units): $\mu_0 = 2.127176 \times 10^{-6}$; $\Delta E = 2.511 \times 10^{-3}$ ($\equiv 551 \text{ cm}^{-1}$); $v = 5.93 \times 10^{-4}$ (at $T = 308 \text{ K}$); $\beta[\frac{1}{2}, (n-1)/2] = 1.255$ (for $n = 5.46$), yielding

$$\lambda = 2.06 \times 10^{-1} C_n^2. \quad (24)$$

Equation (21) represents the magnetic-field dependence of the transition probability as a function of b , and leads to the following expression for the Zeeman mixing cross section $Q(\frac{1}{2}, -\frac{1}{2} \rightarrow \frac{1}{2}, \frac{1}{2})$:

$$Q = \pi R_0^2 P(R_0) + 2\pi \int_{R_0}^{\infty} b db P(b) = \pi R_0^2 \frac{n_1}{n_1 - 2} \frac{\lambda B^2}{R_0^{n_1}}, \quad (25)$$

where R_0 is the classical hard-core radius. As an essential correction to the straight-path approximation, collision partners do not penetrate within R_0 and, accordingly, the integration in Eq. (25) is carried out from R_0 to ∞ . The transition probability at smaller impact parameters is assumed equal to that at $b = R_0$. Equation (25) also indicates that Q has a quadratic dependence on B . There is still, however, the second-order perturbation term, the third term in Eq. (12), which contributes a field-independent part to the cross section Q . The relevant matrix elements between the Zeeman substates of ${}^2P_{3/2}$, with $m = \pm\frac{3}{2}, \pm\frac{1}{2}$, are

$$\begin{aligned} & \langle 2 | V^I(t_1) V^I(t_2) | 1 \rangle \\ &= \sum_m \langle 2 | V^I(t_1) | \frac{3}{2}, m \rangle \langle \frac{3}{2}, m | V^I(t_2) | 1 \rangle. \end{aligned} \quad (26)$$

Bearing in mind the weakness of the magnetic coupling in Eqs. (3) and (4), we note that the major part of each term in Eq. (26) is given by the field-independent expression

$$\begin{aligned} & \langle 2 | V^I(t_1) | \frac{3}{2}, m \rangle \langle \frac{3}{2}, m | V^I(t_2) | 1 \rangle \\ & \approx \langle \frac{1}{2}, \frac{1}{2} | V^I(t_1) | \frac{3}{2}, m \rangle \langle \frac{3}{2}, m | V^I(t_2) | \frac{1}{2}, -\frac{1}{2} \rangle. \end{aligned} \quad (27)$$

From Eq. (9),

$$\begin{aligned} & \langle \frac{1}{2}, \frac{1}{2} | V^I(t_1) | \frac{3}{2}, m \rangle \langle \frac{3}{2}, m | V^I(t_2) | \frac{1}{2}, -\frac{1}{2} \rangle \\ &= \exp[i\Delta E(t_1 - t_2)] \langle \frac{1}{2}, \frac{1}{2} | V^I(t_1) | \frac{3}{2}, m \rangle \\ & \quad \times \langle \frac{3}{2}, m | V^I(t_2) | \frac{1}{2}, -\frac{1}{2} \rangle, \end{aligned} \quad (28)$$

which describes virtual transitions from the ${}^2P_{1/2, -1/2}$ state to the ${}^2P_{3/2}$ Zeeman substates and then to the ${}^2P_{1/2, 1/2}$ state, induced by collisions without the participation of the magnetic field. The transition probability can be calculated as a function of the impact parameter b , to give the field-independent cross section Q_0 . At fields where TDPT is valid, the probabilities (rather than the transition amplitudes) of the field-dependent and field-independent parts may be summed because the interference term becomes negligible after averaging over all orientations. Thus the total cross section Q_T is

$$Q_T = Q_0 + Q = C_2 + C_1 B^2, \quad (29)$$

$$C_1 = \pi \frac{n_1}{n_1 - 2} \frac{\lambda}{R_0^{n_1 - 2}}, \quad C_2 = Q_0. \quad (30)$$

In principle, C_1 and C_2 can be evaluated if the interaction potential and R_0 are accurately known, but given the uncertainties of the theoretical potentials for small impact parameters as well as the approximations inherent in the classical-path approach, it is preferable to derive C_1 and C_2 from experimental data and in this way obtain constraints on V and R_0 .

We note that, in the absence of the magnetic field, a collisional transition from the ${}^2P_{1/2, -1/2}$ state directly to the ${}^2P_{1/2, 1/2}$ state is forbidden by the "instantaneous" time-reversal symmetry selection rule; transitions can take place only through channels involving virtual transitions to the ${}^2P_{3/2, m}$ states, as shown by Eq. (27). However, the magnetic field breaks the time-reversal symmetry by coupling the ${}^2P_{1/2}$ state to the ${}^2P_{3/2}$ state and thus enhances the ${}^2P_{1/2, -1/2} \leftrightarrow {}^2P_{1/2, 1/2}$ transitions. Even though the coupling constant α is small ($\alpha = 4 \times 10^{-4}$ at $B = 1 \text{ T}$), the enhancement of the transitions is by no means negligible if one considers the rapidly oscillating phase factors in Eq. (28), compared to the essentially static one in Eq. (17). The magnetic-field-enhanced probability for the ${}^2P_{1/2}$ Zeeman transitions, relative to the field-independent term, can be considerably larger than $|\alpha|^2$, and as shown below, a substantial enhancement of the cross section was found experimentally.

The quadratic dependence of Q on B given in Eq. (25) is modified by saturation effects at high fields. At high fields, perturbation theory breaks down and can give unphysically large results if not constrained by the uncertainty of the scattering matrix, and indeed, the probability in Eq. (21) can exceed 1 at higher fields and small impact parameters. However, the first-order Magnus approximation [1], together with the evaluation of Eq. (14), shows that the size of $P(b)$ is limited to $P(b) \leq \frac{3}{5}$ by the geometry of spin-orbit coupling after averaging over collisional orientation. For strong collisions $P(b)$ oscillates between this maximum and zero, with an average value $\frac{3}{10}$. This limit affects the field-dependence of Q by re-

stricting the enhancement of the cross section at high field strengths. The cross section may now be expressed as

$$Q = \pi b_0^2 P(b_0) + 2\pi \int_{b_0}^{\infty} b db P(b) = \pi b_0^2 \frac{n_1}{n_1 - 2} \frac{\lambda B^2}{b_0^{n_1}}, \quad (31)$$

where b_0 , which had replaced R_0 in Eq. (25), satisfies the condition

$$P(b_0) = \frac{\lambda B^2}{b_0^{n_1}} = 0.3. \quad (32)$$

Substitution of Eq. (32) into (31) gives the field-induced enhancement Q' of the cross section at the 0.3 probability limit,

$$Q' = \pi \frac{n_1}{n_1 - 2} \frac{3}{10} \left[\frac{\lambda B^2}{0.3} \right]^{2/n_1}. \quad (33)$$

Equation (33) indicates that, when $n = 5.46$ [$n_1 = 2(n - 1) = 8.92$], Q' is proportional to $B^{0.45}$, replacing the quadratic dependence on B at lower fields. The corresponding total cross section Q_T is given by

$$Q_T = Q_0 + Q' = Q_0 + C_1' B^{2/n_1}, \quad (34)$$

with C_1' defined as

$$C_1' = \pi \frac{n_1}{n_1 - 2} \frac{3}{10} \left[\frac{\lambda}{0.3} \right]^{1/n_1}. \quad (35)$$

It may be seen from the above that the theory predicts a change in the B dependence of the cross section Q at a limiting magnetic-field strength, which can also be stated in terms of R_0 and the adjustable parameter C_1 . The transition point of the field, B_{TP} , at which the dependence of Q' on B changes from quadratic to B^{2/n_1} , may be expressed as

$$\frac{\lambda B_{TP}^2}{R_0^{n_1}} = 0.3. \quad (36)$$

λ is related to the adjustable parameter C_1 by Eq. (30) and, using Eqs. (36) and (37), B_{TP} can be expressed in terms of C_1 and R_0 :

$$B_{TP} = \left[\frac{3\pi}{10} \frac{n_1}{n_1 - 2} \frac{R_0^2}{C_1} \right]^{1/2}. \quad (37)$$

As the result of this calculation it is possible to predict the general form of the B dependence of the ${}^2P_{1/2}$ Zeeman mixing cross section Q_T and of the ${}^2P_{1/2}$ disorientation cross section $\sigma_{1/2}^{(1)}$, where

$$\sigma_{1/2}^{(1)} = 2Q_T. \quad (38)$$

Thus

$$Q_T = \begin{cases} Q_0 + C_1 B^2, & B < B_{TP} \\ Q_0 + C_1' B^{0.45}, & B \geq B_{TP} \end{cases} \quad (39)$$

$$Q_T = \begin{cases} Q_0 + C_1 B^2, & B < B_{TP} \\ Q_0 + C_1' B^{0.45}, & B \geq B_{TP} \end{cases} \quad (40)$$

Equation (40) is an oversimplification of the saturation effect at high fields, since it is the total average transition probability (field-independent as well as field-dependent) which is constrained by unitarity and geometry. Therefore, the field-independent contribution Q_0 should be cancelled at high fields. Unfortunately, the field dependence of the cancellation depends on the variation of the field-independent transition probability with the impact parameter, and its computation was beyond the scope of the present calculation.

B. Derivation of the ${}^2P_{1/2}$ Zeeman mixing cross section from the relative intensities of the Zeeman fluorescence components

When Cs vapor containing atoms excited to the $6^2P_{1/2}$ state is placed in a magnetic field, the $6^2P_{1/2}$ and $6^2S_{1/2}$ states are split into magnetic (Zeeman) sublevels, as shown in Fig. 1. The sublevels correspond to substates denoted by magnetic quantum numbers m_J . Although each substate can be further split into hyperfine structure components due to nuclear spin, the nuclear spin is well decoupled at $B > 0.1$ T [11] and does not contribute significantly to the mixing of the Zeeman substates at higher fields.

Collisions between the excited Cs atoms in their Zeeman substates and He atoms cause Zeeman mixing, described by the following equation:

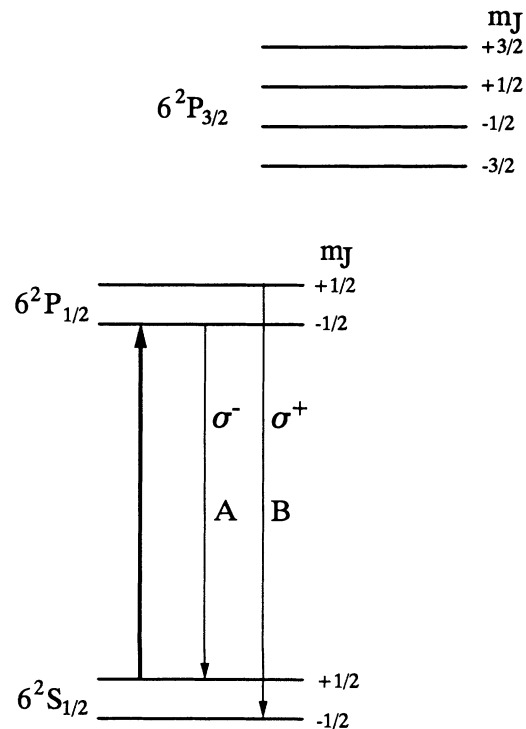
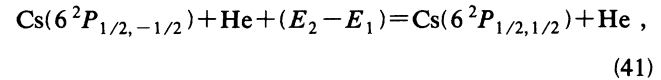


FIG. 1. Partial energy-level diagram for Cs showing 6^2P Zeeman splitting. Collisional mixing takes place only between the ${}^2P_{1/2}$ Zeeman substates. The separations between the levels are not drawn to scale, the π transitions are not shown.

where $\text{Cs}(6^2P_{1/2,-1/2})$ and $\text{Cs}(6^2P_{1/2,1/2})$ are Cs atoms in their two Zeeman substates, and He is a ground-state He atom. $E_2 - E_1$ is the energy difference between the two substates $m_J = \frac{1}{2}$ and $m_J = -\frac{1}{2}$, the magnitude of which depends on the magnetic field strength. Real collisional transitions between the $6^2P_{1/2}$ and $6^2P_{3/2}$ fs states are neglected because of the large fine-structure splitting (551 cm^{-1}).

When the $6^2P_{1/2,-1/2}$ state is populated by laser excitation, the time evolution of the two Zeeman substates may be described by the rate equations

$$\frac{dn_-}{dt} = S_-(t) - \frac{n_-}{\tau} - Z_{-1/2,1/2}n_- + Z_{1/2,-1/2}n_+, \quad (42)$$

$$\frac{dn_+}{dt} = -\frac{n_+}{\tau} + Z_{-1/2,1/2}n_- - Z_{1/2,-1/2}n_+. \quad (43)$$

$S_-(t)$ is the excitation rate of the $m_J = -\frac{1}{2}$ state; n_- , n_+ are the densities of the atoms in the $m_J = -\frac{1}{2}$ and $m_J = +\frac{1}{2}$ substates, respectively; $Z_{-1/2,1/2}$ and $Z_{1/2,-1/2}$ are the collision numbers (defined as numbers of collisions per excited and oriented atom per second) corresponding to the transitions within the $2P_{1/2}$ state, $m_J = -\frac{1}{2} \rightarrow m_J = \frac{1}{2}$ and $m_J = \frac{1}{2} \rightarrow m_J = -\frac{1}{2}$. At fields $B \ll kT/\mu_0 \approx 430 \text{ T}$, $Z_{-1/2,1/2} \approx Z_{1/2,-1/2} \equiv Z$. Furthermore, $\tau = 34 \text{ ns}$ is the average lifetime of the $2P_{1/2}$ state [15]. The general solutions of Eqs. (42) and (43) are

$$n_{\pm}(t) = \frac{1}{2} \int_0^{\infty} e^{-u/\tau} (1 \mp e^{-2Zu}) S_-(t-u) du, \quad (44)$$

where it is assumed that $n_{\pm}(-\infty) = 0$.

The observed integrated populations are

$$N_{\pm} = \int_{t_0}^{\infty} n_{\pm}(t) dt. \quad (45)$$

The integration is carried out from t_0 instead of $-\infty$ because a (gating) delay time t_0 between the exciting laser pulse and the detection of the fluorescence was applied in the experiment to avoid scattered laser light. The explicit expression for the integrated population is therefore

$$N_{\pm} = \frac{1}{2} \int_{t_0}^{\infty} dt \int_0^{\infty} du e^{-u/\tau} (1 \mp e^{-2Zu}) S_-(t-u). \quad (46)$$

The average excitation rate may be approximated by a Gaussian:

$$S_-(t) = S_1(0) e^{-t^2/\Delta^2}. \quad (47)$$

The effective e^{-1} half-width Δ of the exciting laser pulse was measured to be 3.4 ns .

The measured fluorescence counts (or integrated intensities), I_- and I_+ for σ^- and σ^+ transitions, respectively, are proportional to the products of the integrated populations and the Einstein A coefficients:

$$I_- = AN_-; \quad I_+ = AN_+. \quad (48)$$

The same A coefficient is used for both transitions as the A coefficients for the σ^- and σ^+ transitions are very nearly equal to one another [16]. The measured intensity

ratio η is defined as

$$\eta = \frac{I_+}{I_-} = \frac{N_+}{N_-}. \quad (49)$$

Equations (46), (47), and (49) yield

$$\eta = \frac{1 + 2Z\tau - \exp(-2Zt')}{1 + 2Z\tau + \exp(-2Zt')}, \quad (50)$$

where $t' = t_0 - Z\Delta^2/2$ and t_0 is the delay time. The delay time was measured to be approximately 30 ns . The Zeeman (total) mixing cross section Q_T is defined analogously with the gas-kinetic cross section:

$$Z = NQ_T v_r. \quad (51)$$

Q_T is the cross section for transition between $P_{1/2}$ Zeeman sublevels, N is the density of the He atoms, and v_r is the average relative speed of the colliding atoms whose reduced mass is μ .

$$v_r = (8kT/\pi\mu)^{1/2}. \quad (52)$$

k is the Boltzmann constant and T is the absolute temperature of the vapor-gas mixture.

The exponential term in Eq. (50) is expanded to yield an approximate expression for η :

$$\eta \approx Z(\tau + t') - Z^2\tau^2 + Z^3\tau^3 \left[1 - \frac{t'}{\tau} - \frac{(t')^2}{\tau^2} - \frac{(t')^3}{3\tau^3} \right] - \dots, \quad (53)$$

which reduces to the following expression that contains terms up to the second order of $(Z\tau)^2$:

$$\eta \approx Z(\tau + t_0) - Z^2(\tau^2 + \Delta^2/2). \quad (54)$$

Careful consideration was given to the spread of the delay time (jitter), since some of the detected pulses were delayed more than others as they passed through the detection electronics (the photomultiplier and the gated pulse sampler). The result was a distribution of detected pulses with different delays t_0 relative to the excitation-pulse maximum before the particular group of pulses began to be counted. The expressions for N_{\pm} can be averaged over this distribution (assumed to be Gaussian) and the final corrected expression for η is

$$\eta = Z \left[\tau + t_0 - \frac{\delta^2}{2\tau} \right] - Z^2 \left[\tau^2 + \frac{1}{2}(\Delta^2 + \delta^2) \right], \quad (55)$$

where δ is the jitter (ns).

Equation (55), together with $Z = NQ_T(\frac{1}{2}, -\frac{1}{2} \rightarrow \frac{1}{2}, \frac{1}{2})v_r$, provides the connection between the measured relative intensities of the fluorescence components and the cross section $Q_T(\frac{1}{2}, -\frac{1}{2} \rightarrow \frac{1}{2}, \frac{1}{2})$.

III. EXPERIMENTAL DETAILS

The arrangement of the apparatus is shown schematically in Fig. 2. Cesium or rubidium vapor, contained together with helium in a quartz cell, was located in a mag-

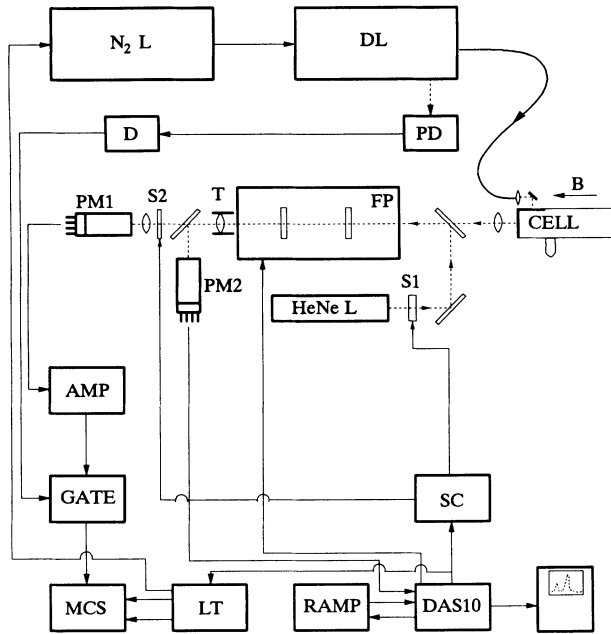


FIG. 2. Schematic diagram of the apparatus. N_2L , nitrogen laser; DL, dye laser; PD, photodiode; D, delay line; FP, Fabry-Pérot interferometer; T, telescope; PM1, PM2, photomultipliers; S1, S2, shutters; AMP, amplifier-discriminator; GATE, gated pulse-inverter amplifier; LT, channel advance laser trigger; RAMP, ramp voltage generator; DAS10, FP stabilizer; SC, shutter controller. B indicates the magnetic field.

netic field that could be varied in the range 0–7 T. Radiation from a pulsed dye laser was used to produce selective excitation of the $n^2P_{1/2}$ ($m_J = -\frac{1}{2}$) Zeeman substate ($n=5$ for Rb and 6 for Cs). The resulting fluorescence spectrum was monitored along the direction of the magnetic field and perpendicularly to the direction of excitation, resolved with a scanning Fabry-Pérot (FP) interferometer, detected with a photomultiplier (PM) tube, and accumulated in a multichannel scaler (MCS).

The two-stage dye laser was pumped with a N_2 laser at a repetition rate of about 12 Hz and produced light pulses of about 7 ns in width. In the Rb experiment the dye laser was operated with Oxazine 750 at 794.76 nm and IR-125 was used in the Cs experiment, producing output at 894.35 nm. Both dyes (supplied by the Exciton Corp.) were dissolved in dimethylsulphoxide (DMSO) at a concentration of about $1.7 \times 10^{-3} M$. The dye-laser output had a bandwidth of about 0.04 nm and was scanned by a stepper motor with a resolution of 8×10^{-3} nm per step. The long-term stability of the output was better than 0.05 nm per day, and once a day the output wavelength was checked against a thermionic diode. The radiation from the dye laser was conveyed to the vapor cell by an optical fiber.

The quartz vapor cell was mounted in an oven heated by oil circulating from a Neslab ultrathermostat, which maintained the cell at 35°C during the Cs experiment and at 65°C during the Rb experiment. The cell was fitted with a side arm containing an excess of the metal, which was heated separately and was kept at a temperature

about 2° below that of the fluorescing region in the vapor-gas mixture. The cell was connected by a narrow-bore tube and a greaseless stopcock to a vacuum and gas filling system from which helium (Matheson, research grade) was admitted as required. Gas pressures were measured with an MKS Baratron capacitance gauge.

The fluorescence emitted by the vapor-gas mixture was collected and rendered parallel by a lens placed in front of the piezoelectrically scanned FP interferometer (Burleigh Model No. 110) which was scanned at 0.5 Hz and was stabilized using a He-Ne laser as a reference. The interferometer resolved the fluorescence spectrum and its output was focused on the photocathode of the ITT FW118 refrigerated PM tube whose output pulses were amplified by an Ortec Model No. 9302 amplifier-discriminator. The resulting signal was gated and registered in the channels, corresponding to the FP scan, of a 1024-channel MCS from which the accumulated spectrum was transferred to a personal computer where the integrated relative intensities of the fluorescence components were determined after correction for background noise counts. The gating delay was about 30 ns and the gate was open for 640 ns.

Before each experimental run performed at a different magnetic field strength, the free spectral range of the interferometer was checked to ensure that the peaks arising from the direct and the collisionally induced fluorescence were properly resolved. A scan at zero He pressure was made to confirm the absence of the collisionally induced fluorescence and thus the negligible frequency of Cs-Cs (or Rb-Rb) collisions. At each field strength the experiment was carried out with several He pressures ranging from zero to 5 Torr. About 1000 scans of the interferometer were made at each of the higher He pressures, and about 2000 scans at the lower He pressures, recording sufficient data for an acceptable signal-to-noise ratio.

IV. RESULTS AND DISCUSSION

Figures 3 and 4 show representative traces of the $^2P_{1/2}$ fluorescence spectra for Cs at 3 T, and Rb at 7 T, respectively, for various He pressures. The peaks are labeled to correspond to the transitions shown in Fig. 1. Figure 5 shows representative plots of the fluorescence intensity ratios η for Cs against He pressure. For the sake of clarity, only six plots are shown although experimental runs were performed at nine magnetic field strengths. The Rb experiments were carried out at seven different field strengths and gave rise to plots of similar appearance as those in Fig. 5. It may be seen that all the plots in Fig. 5 pass through the origin, indicating the absence of collisionally induced fluorescence at zero He pressure. The intensity ratios are connected to the cross sections Q_T by Eq. (55) which is more explicitly written as

$$\eta = Q_T N v_r \tau \left[1 + \frac{t_0}{\tau} - \frac{\delta^2}{2\tau^2} \right] - (Q_T N v_r \tau)^2 \left[1 + \frac{\Delta^2 + \delta^2}{2\tau^2} \right], \quad (56)$$

where $t_0 = 30$ ns is the delay time measured from the center of the exciting laser pulse, $\tau = 34$ ns for Cs $6^2P_{1/2}$

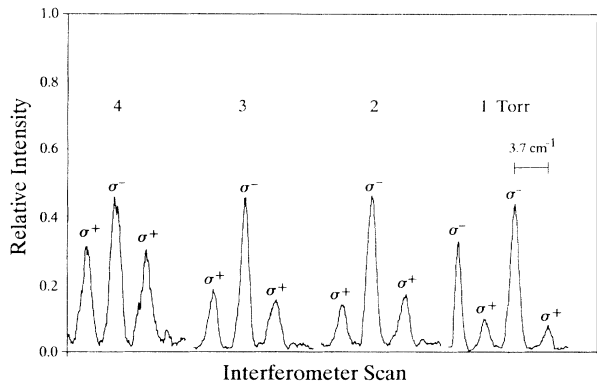


FIG. 3. Piezoelectrically scanned interferogram of the Zeeman fluorescence spectrum of the Cs $6^2P_{1/2}$ state, emitted from a Cs-He mixture at various He pressures. The $6^2P_{1/2}$ ($m_J = -\frac{1}{2}$) Zeeman state was excited with laser light and the peaks correspond to the transitions indicated in Fig. 1. $B = 3$ T.

and 28 ns for Rb $5^2P_{1/2}$ [15], $\Delta = 3.5$ ns is the half width of the exciting pulse, and $\delta = 15$ ns is the jitter half width. $Nv_r\tau$ is a function of the pressure P and temperature T of helium. If the gas is assumed to be ideal,

$$Nv_r\tau = 2.42 \times 10^{19} P / \sqrt{T} m^{-2} \quad (57)$$

with P measured in Torr and T in kelvin. The Cs measurements were carried out at $T = 308$ K and the Rb measurements at 338 K. Substitution of the experimental t_0 , Δ , and δ values in Eq. (57) yielded

$$\eta = Q_T Nv_r\tau (1.76 \pm 0.18) - (Q_T Nv_r\tau)^2 (1.10 \pm 0.03). \quad (58)$$

The curves in Fig. 5 represent least-mean-square fits of Eq. (58) to the experimental data, with Q_T as the adjustable parameter. It may be seen that the fit to the experimental data is quite good, confirming the validity of Eq. (56).

As stated in Sec. II, Gaussian time evolution of the ex-

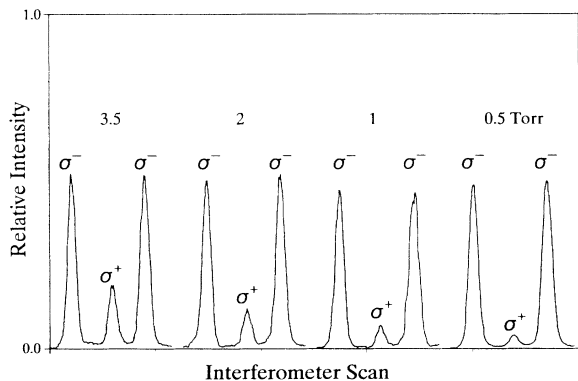


FIG. 4. Piezoelectrically scanned interferogram of the Zeeman fluorescence spectrum of the Rb $5^2P_{1/2}$ state, emitted from a Rb-He mixture at various He pressures and with $B = 7$ T. The $5^2P_{1/2}$ ($m_J = -\frac{1}{2}$) Zeeman state was excited with laser light and the peaks correspond to the transitions indicated in Fig. 1.

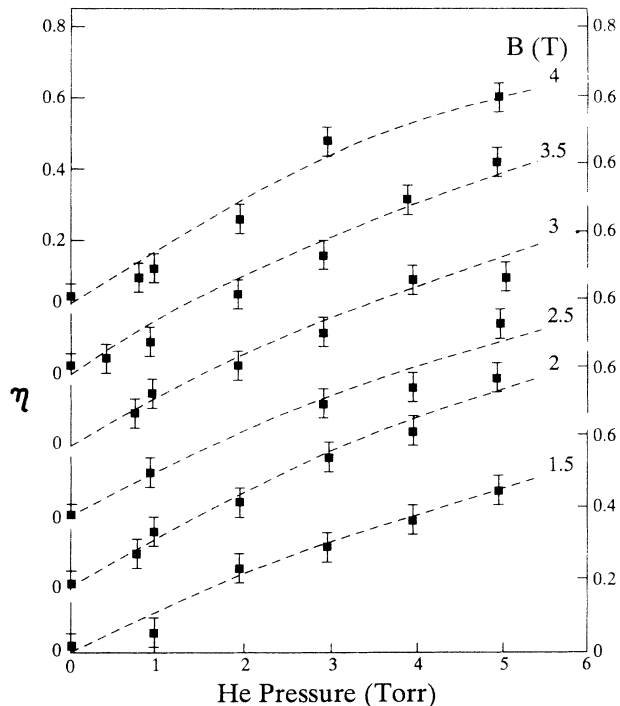


FIG. 5. Plots of Zeeman fluorescence intensity (and population) ratios, showing effects of Zeeman mixing induced in Cs-He collisions following $6^2P_{1/2}$ ($m_J = -\frac{1}{2}$) excitation. The separate origin for each plot is indicated on the vertical axis. The dashed curves are plots of Eq. (56).

iting laser pulse was used as a convenient approximation to produce an analytic solution of the rate equations (42) and (43). The rate equations were also solved numerically using the experimentally determined time evolution of the laser pulse, and the agreement between the two solutions was very good. Consequently we used the analytic solution [Eq. (58)] in the data analysis. The cross sections Q_T for Zeeman mixing in Cs $6^2P_{1/2}$, yielded by the fitting procedure, obtained for nine values of the magnetic field strength, are plotted against B in Fig. 6 together with the

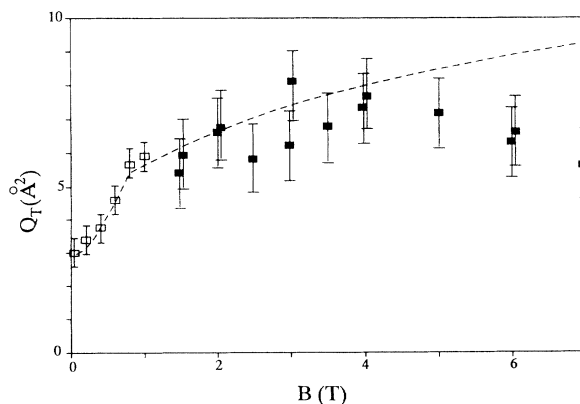


FIG. 6. Variation of the Cs $6^2P_{1/2}$ Zeeman mixing cross section with magnetic field. The points represent experimental measurements, the dashed line represents the theoretical calculation [Eqs. (59) and (60)].

previously reported low-field data [10]. The plot indicates a general increase of Q_T with B , confirming the enhancement effect of the magnetic field. It is apparent in Fig. 6 that there are two separate regions in the Q_T-B variation, joined at a “transition point” where $B_{TP}=0.76$ T. This value, when substituted in Eq. (37), produced the classical “hard-core” collision radius $R_0=2.8a_0$, where a_0 is the Bohr radius, a value close to the previously calculated result of $3.2 a_0$ [17]. $R_0=2.8a_0$ was substituted in Eq. (35) yielding $C'_1=0.67$ a.u. These results, obtained from a one-point fit of Eq. (40) to the experimental data, make it possible to represent the variation of Q with B :

$$Q_T = \begin{cases} 10.7 + 14.6B^2 \text{ a.u.} = 3 + 4.1B^2 \text{ \AA}^2, & B < 0.76 \text{ T} \\ 10.7 + 9.67B^{0.45} \text{ a.u.} = 3 + 2.71B^{0.45} \text{ \AA}^2, & B \geq 0.76 \text{ T} \end{cases} \quad (59)$$

$$Q_T = \begin{cases} 10.7 + 14.6B^2 \text{ a.u.} = 3 + 4.1B^2 \text{ \AA}^2, & B < 0.76 \text{ T} \\ 10.7 + 9.67B^{0.45} \text{ a.u.} = 3 + 2.71B^{0.45} \text{ \AA}^2, & B \geq 0.76 \text{ T} \end{cases} \quad (60)$$

Equations (59) and (60) are also plotted in Fig. 6 together with the experimental results, and it may be seen that there is good agreement between the calculated and experimental data in the range $0 < B < 5$ T. At $B > 5$ T the experimental measurements suggest the tendency of the field-mediated transition to cancel the field-independent transitions at high fields, as mentioned at the end of Sec. II A. It is intended to pursue the calculation further and examine the field dependence of the cancellation effect.

The experimental and theoretical data also provide information on the Cs-He interaction. The coefficient C_n was calculated by substituting $\lambda=3.14 \times 10^3$ in Eq. (24) which gave $C_n=1.23 \times 10^2$, and Eq. (20) produced the repulsive interaction potential involved in the Cs-He collision:

$$V(R)=1.23 \times 10^2 R^{-5.46} \text{ a.u.} \quad (61)$$

This potential differs from an earlier version $V(R)=1.12 \times 10^3 R^{-5.46}$ a.u. which was obtained from a power-series fit to computed potentials [1,17]. Q_0 resulted from the inclusion of second-order perturbation which, presumably, gave a more correct and accurate potential that is somewhat “soft” and permits a smaller “hard-core” collision radius.

The Zeeman mixing cross section for collisions of $5^2P_{1/2}$ Rb atoms with He was also determined over the range of magnetic fields using the same experimental method in conjunction with Eq. (58) in which τ represented the lifetime of 5^2P Rb atoms. As may be seen in Fig. 7, there appears to be no enhancement of the Zeeman mixing cross section, and the cross section remains constant within experimental error throughout the range of the magnetic field strength from 1 to 7 T. We did not measure the cross section at $B < 1$ T or at $B=0$ which had been done in this laboratory for Cs [18], yielding data consistent with the intermediate- and high-field measurements. One might expect that at $B=0$ the cross section

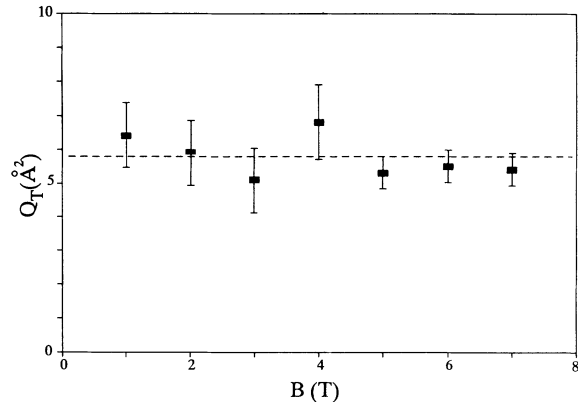


FIG. 7. Rb $5^2P_{1/2}$ Zeeman mixing cross section measured at $1 \text{ T} \leq B \leq 7 \text{ T}$. The dashed line indicates the constant average value of the cross section.

for Rb might be somewhat smaller than at $B \geq 1$ T, though in Rb the $P_{1/2}-P_{3/2}$ fine-structure splitting is less than half as large as in Cs, and it is possible that considerable collisional “virtual mixing” between the fine-structure states may take place at $B=0$, with the system already becoming saturated at 1 T. According to Eqs. (23), (30), and (37), B_{TP} for Rb should be less than half of the Cs value. Theory would predict Q_0 to be significantly larger for Rb than for Cs whereas the saturated values of Q_T at high fields are quite similar. It is difficult to compare the high-field cross sections with other data since several experimental and theoretical low-field and zero-field cross sections have been reported in the past, with widely differing values which are collected in Table I. We note that our cross section $Q_T=5.8 \text{ \AA}^2$ is in good agreement with two of the calculations [19,24] though it is smaller than the other experimental values.

V. SUMMARY AND CONCLUSIONS

We have carried out an experimental and theoretical investigation of the magnetic-field dependence of the Zeeman mixing cross section for collisions of oriented Cs $6^2P_{1/2}$ atoms with ground-state He atoms, over a range $1 \text{ T} \leq B \leq 7 \text{ T}$. The collisional interaction of Cs atoms with He atoms at thermal energies was studied by selectively

TABLE I. Cross sections for $5^2P_{1/2}$ Zeeman mixing in Rb induced by He collisions.

$Q_T(\frac{1}{2}, -\frac{1}{2} \leftrightarrow \frac{1}{2}, \frac{1}{2})$ (\AA^2)	Method	Magnetic-field strength (T)	Source
5.8	Expt.	1–7	This work
16.6	Expt.	0.11	Ref. [20]
11.5	Expt.	0	Ref. [21]
6.6	Theor.	0	Ref. [19]
12.6	Theor.	0	Ref. [22]
17.0	Theor.	0	Ref. [23]
7.0	Theor.	0	Ref. [24]

exciting the Cs $6^2P_{1/2, -1/2}$ Zeeman state by laser radiation and measuring the relative intensities of the two fluorescence components arising from the directly excited $m = -\frac{1}{2}$ and collisionally populated $m = +\frac{1}{2}$ states. The experimentally determined field dependence of the cross section is shown in Fig. 6, together with the theoretically predicted dependence calculated using time-dependent perturbation theory to second order, which also yielded the Cs-He interaction potential. Both the experimental and the theoretical results show the enhancement of the cross section by the magnetic field and are in good agree-

ment over the range $1 \text{ T} \leq B \leq 5 \text{ T}$. A similar experimental study of the $5^2P_{1/2}$ Rb Zeeman mixing cross section over the range $1 \text{ T} \leq B \leq 7 \text{ T}$ indicates no magnetic-field enhancement of the cross section, as indicated in Fig. 7.

ACKNOWLEDGMENT

This research was supported by a grant from the Natural Sciences and Engineering Research Council of Canada.

-
- [1] References to most of the earlier work, that was largely restricted to alkali-metal atoms, may be found in W. E. Baylis, in *Progress in Atomic Spectroscopy, Part B*, edited by W. Hanle and H. Kleinpoppen (Plenum, New York, 1979).
 - [2] M. Kimura, H. Kato, K. Someda, and H. Nakamura, *J. Chem. Phys.* **96**, 7423 (1992).
 - [3] R. W. Berends, W. Kedzierski, and L. Krause, *Phys. Rev. A* **37**, 68 (1988).
 - [4] W. Kedzierski, R. B. Middleton, and L. Krause, *Phys. Rev. A* **43**, 143 (1991).
 - [5] J.-M. Mestdagh, P. Meynadier, P. de Pujo, O. Sublemontier, J.-P. Visticot, J. Berlande, J. Cuvelier, T. Gustavsson, A. G. Suits, and Y. T. Lee, *Phys. Rev. A* **47**, 241 (1993).
 - [6] X. L. Han and G. W. Schinn, *Phys. Rev. A* **43**, 266 (1991).
 - [7] J. C. Gay and W. B. Schneider, *Phys. Rev. A* **20**, 905 (1979).
 - [8] J. C. Gay and W. B. Schneider, *Phys. Rev. A* **20**, 894 (1979).
 - [9] S. Matsumoto, K. Shiozawa, Y. Ishitani, A. Hirabayashi, and T. Fujimoto, *Phys. Rev. A* **44**, 4316 (1991).
 - [10] J. Guiry and L. Krause, *Phys. Rev. A* **12**, 2407 (1975).
 - [11] Ju Gao, M.Sc. thesis, University of Windsor, 1993 (unpublished).
 - [12] W. E. Baylis, *J. Chem. Phys.* **51**, 2665 (1969).
 - [13] W. E. Baylis, in *Progress in Atomic Spectroscopy, Part A*, edited by W. Hanle and H. Kleinpoppen (Plenum, New York, 1978).
 - [14] *Handbook of Mathematical Functions*, edited by M. Abramowitz and I. A. Stegun (Dover, New York, 1964).
 - [15] J. K. Link, *J. Opt. Soc. Am.* **56**, 1195 (1966).
 - [16] A. C. G. Mitchell and M. W. Zemansky, *Resonance Radiation and Excited Atoms* (Cambridge University, Cambridge, England, 1934).
 - [17] W. E. Baylis (unpublished).
 - [18] B. Niewitecka and L. Krause, *Can. J. Phys.* **54**, 748 (1976).
 - [19] E. P. Gordeyev, E. E. Nikitin, and M. Ya Ovchinnikova, *Can. J. Phys.* **47**, 1819 (1969).
 - [20] B. Kamke, *Z. Phys. A* **273**, 23 (1975).
 - [21] B. R. Bulos and W. Happer, *Phys. Rev. A* **4**, 849 (1971).
 - [22] E. Roueff and A. Suzor, *J. Phys. (Paris)* **35**, 727 (1974).
 - [23] J. Pascale (unpublished).
 - [24] B. Bruillaud and R. Gayet, *J. Phys. B* **10**, 2143 (1977).